Journal of Power Sources 195 (2010) 195–203

Contents lists available at ScienceDirect

Journal of Power Sources

journal homepage: www.elsevier.com/locate/jpowsour

Thermal stability of a new solid oxide fuel/electrolyzer cell seal glass

T. Jin, K. Lu*

Department of Materials Science and Engineering, Virginia Polytechnic Institute and State University, Blacksburg, VA 24061, USA

ARTICLE INFO

Article history:
Received 12 June 2009
Received in revised form 11 July 2009
Accepted 13 July 2009
Available online 21 July 2009

Keywords:
Thermal stability
Seal glass
Devitrification
Atmosphere
Nucleation
Solid oxide fuel/electrolyzer cells

ABSTRACT

Long-term thermal stability of sealing glass is critical for hermetic seals of solid oxide fuel and electrolyzer cell stacks. In this work, a $SrO–La_2O_3–Al_2O_3–SiO_2$ glass (SABS-0 glass) has been evaluated as a high temperature sealant by thermal treatment. Powder and bulk SABS-0 glasses are studied in both air and H_2/H_2O atmospheres at 800 °C for up to 1000 h. Weight measurements show negligible SABS-0 glass vaporization during the thermal treatment. Both SABS-0 powder and bulk samples show some surface devitrification but the SABS-0 glass bulk remains amorphous at all the thermal treatment conditions. On the polished bulk SABS-0 surface, needle-shaped crystals are observed for both the air and the H_2/H_2O thermal treatment conditions. Polishing is believed to be the initiator for the SABS-0 glass surface devitrification. The crystalline phases, indentified as silicates and aluminates, increase with the thermal treatment time. However, the crystalline phases on the polished SABS-0 glass surface are very limited and only exist on the very surface of both the air and the H_2/H_2O atmosphere treated samples. The SABS-0 glass has excellent thermal stability in solid oxide fuel/electrolyzer operating environments and is a promising sealant material for such applications.

1. Introduction

High temperature sealing material plays a vital role in the performance of energy conversion devices such as solid oxide fuel cells (SOFCs) and solid oxide electrolyzer cells (SOECs) [1]. Glass and glass–ceramic materials are considered as the most desirable candidates to seal ceramic electrode–metal interconnect and ceramic electrolyte–metal interconnect at high temperatures because of their ability of forming a hermetic seal. Extensive work has been done to develop glass and glass–ceramic seals [2,3]. To be used as a SOFC/SOEC seal, glass should meet several stringent thermal stability requirements. First, it must seal during the entire SOFC/SOEC operation (room temperature to 900 °C) to prevent gas leakage from or mixing in cell stacks [4,5]. Fuel gases (hydrogen or hydrocarbon species) and air must be separated between anode and cathode to avoid energy conversion efficiency decrease, combustion of gases, or local overheating [3,6]. This means no glass vaporization or interaction with any cell atmosphere should occur. Second, a seal must possess long-term stability in a wide range of oxygen partial pressure (fuel gas or air) and wet environment with hundreds of thermal cycles and/or >40,000 operating hours. High devitrification resistance in the above conditions is necessary in order to avoid thermophysical property mismatch at the sealing interfaces [7].

Alkaline earth containing silicate glasses and glass–ceramics have been actively studied for sealing purpose [8–12]. BaO and SrO containing silicate glasses are generally favored because they have wider stability windows [11,13,14]. However, a serious issue is the interfacial reaction between the alkaline earth containing glasses and other cell components [15]. For example, a high content of crystalline phases such as $BaAl_2Si_2O_8$ was observed in BaO-containing glasses after a few hundred hours of cell operation. $BaAl_2Si_2O_8$ has much smaller coefficient of thermal expansion (CTE) and tends to create cracks and gas leakage [16,10]. B_2O_3 has been widely used in seal glass to decrease viscosity. However, vaporization of B_2O_3 was reported, especially in wet environments. Weight loss of borosilicate glass can lead to sealant glass structure collapse [17]. Addition of alkaline oxides such as Na_2O and Li_2O into a seal glass provides high CTE, but glass softening temperature decreases drastically to around 700 °C [18]. This low softening temperature means that the glass can become too flowable during the SOFC/SOEC operation. Sealing strength might also be undesirably low. The high mobility of the alkaline ions can also lead to electrical conductivity increase.

A $SrO–La_2O_3–B_2O_3–Al_2O_3–SiO_2$ glass system has been developed by us as a seal glass for SOFCs/SOECs [19]. The thermal stability and devitrification resistance were studied with different B_2O_3 contents. This glass desirably has 635–775 °C glass transition temperature T_g and 670–815 °C dilatometric softening temperature T_d. The CTE is desirably high at $10.5–11.0 \times 10^{-6}\,K^{-1}$. The effects of B_2O_3 content on the glass network structure and thermal proper-

* Corresponding author at: Department of Materials Science and Engineering, Virginia Polytechnic Institute and State University, 213 Holden Hall, Blacksburg, VA 24061, USA. Tel.: +1 540 231 3225; fax: +1 540 231 8919.
E-mail address: klu@vt.edu (K. Lu).

0378-7753/$ – see front matter © 2009 Elsevier B.V. All rights reserved.
doi:10.1016/j.jpowsour.2009.07.023

ties have been studied. Local ordering of different glass structural units and the amount of non-bridging oxygen species increase with B_2O_3:SiO_2 ratio. Increase in B_2O_3 content also degrades thermal properties, including T_g and T_d. Microheterogeneity from different glass structural units increases the tendency of devitrification. Boron-free SrO–La_2O_3–Al_2O_3–SiO_2 glass (SABS-0) exhibits excellent combination of thermal properties and thermal stability even after being kept at 850 °C for 200 h [20]. Nickel addition to the SABS-0 glass decreases T_g and increases devitrification tendency, causing degradation of thermal stability [21]. However, longer term thermal stability of the SABS-0 glass has not been studied.

Currently, seal glasses are mostly applied to the cell stacks in powder format, such as by tape casting. However, seal glass evaluations are mostly carried out for bulk glass. Because the seal glasses are studied at different formats, thermal stability results are not comparable. In reality, the surfaces of a glass are preferential devitrification sites [22]. Seal glass vaporization (if any) and interfacial interactions with other cell components are proportional to the seal glass surface area. Another significant factor to consider is atmosphere effect on the stability of a seal glass. Not only can the atmospheres in the same cell stack be different (reducing vs. oxidizing), but also SOFCs and SOECs have very different gas compositions for the same interface. Particularly, water steam concentration can be up to 90% for SOEC applications and has caused cell stacks to degrade in about 1000 h at 830 °C [23]. This cell life is only about 10% of that for SOFCs and seal degradation could have been the cause. Na_2O- and CaO-containing silicate glasses were tested for 200 h in H_2–3% H_2O atmosphere, degradation was found in the glass sealant [18]. There was also a weight loss for boron-containing glass in wet and reducing atmospheres [17]. These studies indicate that a seal glass should be evaluated for different atmospheres.

This work was aimed to evaluate the thermal stability of the B_2O_3 free SABS-0 glass as SOFC/SOEC seals in different material formats and atmospheres. The SABS-0 glass samples were prepared in both powder and bulk formats with known surface areas. All the samples were thermally treated at 800 °C for 100, 200, 500, and 1000 h. Air and H_2/H_2O mixture (~50% H_2O vapor) were chosen as the study atmospheres. X-ray diffraction (XRD) has been used to examine devitrified crystalline phase(s), if there is any. Scanning electron microscopy (SEM) has been used to characterize the microstructures of the SABS-0 glass.

2. Experimental procedures

2.1. Sample preparation

SABS-0 glass samples were prepared with conventional glass manufacturing process. $SrCO_3$ (99.9%, Sigma Aldrich, St. Louis, MO), La_2O_3 (99.98%), Al_2O_3 (99.95%), and SiO_2 (99.8%) (all oxides were from Alfa Aesar, Ward Hill, MA) at a designed composition ratio were mixed in a ball mill for overnight. The mixed oxides and carbonate were melted in a platinum crucible in a box furnace (Lindberg, Model No. 51314, Watertown, WI) at 1400 °C for 4 h. The molten glass was quenched into a graphite mold.

The SABS-0 glass bulk samples were made by annealing the quenched SABS-0 glass at 725 °C for 2 h, and cutting and grinding the annealed SABS-0 glass pieces into rectangle shape. The bulk SABS-0 glass pieces used weighted 2.5–4.5 g each. The bulk glass surface was polished with polishing papers and 1 μm size alumina particle suspension to optical finish. The SABS-0 glass powder samples were made by crushing large SABS-0 glass pieces without any annealing in an agate mortar and pestle set and sieved with 100–200 mesh sieves. The glass powder particle size was measured by a laser light scattering analyzer (LA-750, Horiba Ltd., Japan). The average particle size was 147 μm and the standard deviation was

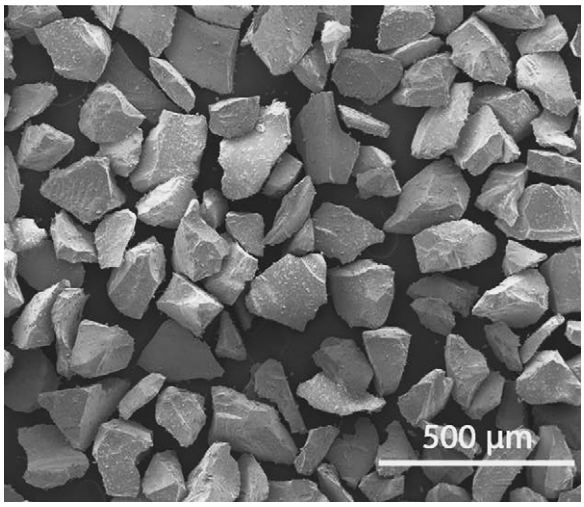

Fig. 1. SEM image of the SABS-0 glass powder used in this study.

62 μm based on six measurements. The SABS-0 glass powder samples used weighted 1–2 g. Fig. 1 shows the image of the as-prepared SABS-0 glass powder. Fig. 2 shows the average particle size distribution; a monomodal particle size distribution is observed.

The surface area of the bulk SABS-0 glass samples was 1.1×10^{-4} to 3.2×10^{-4} $m^2\,g^{-1}$ based on the sample dimension and weight measurements. For the SABS-0 powder samples, the specific surface area was calculated to be 1.1×10^{-2} $m^2\,g^{-1}$ based on the average particle size (assuming particles have spherical shape).

2.2. Thermal treatment

For the SABS-0 glass thermal stability study, both powder and bulk samples were put on platinum foils and heated to 800 °C at the same heating and cooling rate of 3 °C min^{-1} in air and in H_2/H_2O gas mixture. For the thermal treatment in air, the study was carried out in a horizontal tube furnace (Lindberg, Model No. 54233, Watertown, WI). For the thermal treatment in the H_2/H_2O atmosphere, the study was carried out in another horizontal tube furnace (1730-20 HT Furnace, CM Furnace Inc., Bloomfield, NJ). H_2:H_2O ratio was controlled by flowing hydrogen through a water container kept at 83 °C, which was designed to create ~50% water vapor in the gas mixture, based on the vapor pressure of water and the experimental temperature [24]. The H_2/H_2O gas mixture flow rate was $\sim 2 \times 10^{-5}$ $m^3\,s^{-1}$. For both atmospheres, the samples were kept at 800 °C for 100, 200, 500, and 1000 h, respectively.

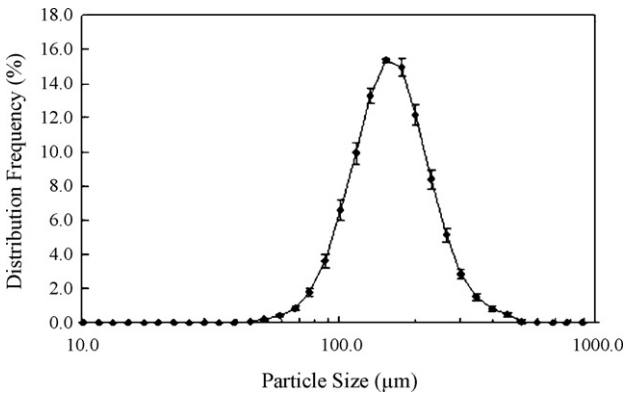

Fig. 2. Particle size distribution of the SABS-0 glass powder.

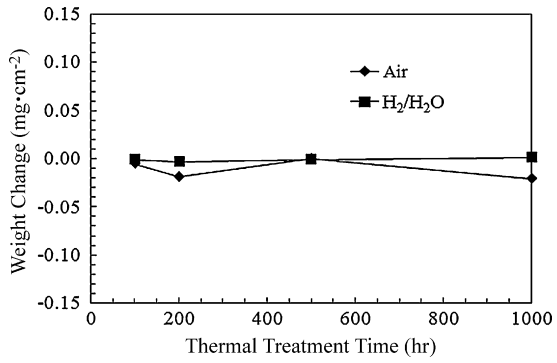

Fig. 3. Weight change of the SABS-0 powder glass thermally treated at 800 °C for different time in air and H_2/H_2O atmospheres.

2.3. Characterization

The weights of the SABS-0 samples before and after the thermal treatment at 800 °C in different atmospheres were measured. Weight loss per unit surface area was calculated.

Microstructural analyses were carried out in a SEM (Quanta 600 FEG, FEI Company, Hillsboro, OR) for both the powder and the bulk samples after different thermal treatment times. XRD studies were carried out for both the powder and the bulk SABS-0 glass samples in an X'Pert PRO Diffractometer (PANalytical B.V., EA Almelo, The Netherlands) to identify the crystalline phase(s) after different thermal treatment conditions. The step size was 0.030° s^{-1} with Cu Kα radiation (λ = 1.5406 Å).

3. Results and discussion

3.1. Weight change of SABS-0 glass

In SOFCs/SOECs, volatile constituents should be avoided or at least have no deleterious effect on cell performances. Concern about vaporization of glass constituents in the long-term use of glass sealants has been raised [25–27]. Borate species are most volatile at 800 °C in dry oxidizing (in $BO_2(g)$) and wet reducing (in $B_3H_3O_6(g)$) atmospheres [17,25]. The reactions can decompose the glass structure and greatly limit the lifetime of a seal. For the SABS-0 glass, this problem has been effectively eliminated since there is no boron species in the composition. However, SiO_2 can potentially vaporize by reacting with water vapor [25]:

$$SiO_2 + H_2O \rightarrow Si(OH)_4 \quad (1)$$

In the SABS-0 glass, there is a substantial amount of SiO_2 (55–60 mol%). In light of the critical function that SiO_2 plays in the SABS-0 glass forming, the glass weight change after long-term thermal treatment has been rigorously evaluated. During the experiments, there was little weight change detected. The only weight difference is on the last digit of the analytical balance (0.0001 g), likely from measurement errors. Since the SABS-0 powder sample has much larger specific surface area than the bulk sample, the weight change measured should be more accurate, if there is any. As shown in Fig. 3, there is very little weight loss or weight gain under both the air and the H_2/H_2O thermal treatment conditions. The maximum weight loss value is 0.02 mg cm^{-2}. This is one to two orders of magnitude lower than that for an alkaline earth silicate glass even though the thermal treatment time is several times longer (168 h vs. 1000 h) [17]. The weight change is too small to be attributed to the SABS-0 glass vaporization. Another confirmation that the SABS-0 glass has negligible weight change is that no trend is observed with the thermal treatment time in Fig. 3. Based on these results, it can be concluded that the weight loss of the SABS-0 glass in the air and the H_2/H_2O atmospheres is negligible at 800 °C.

3.2. Glass microstructure stability

Glass surface devitrification is more common and predominant than bulk devitrification because of higher number of active sites for nucleation [28,29]. For the SABS-0 glass, the sample surfaces should exhibit higher tendency of devitrification than the bulk. Fig. 4 shows the SEM images of the SABS-0 glass powder after 200, 500, and 1000 h of thermal treatment in air at 800 °C. After 200 h of thermal treatment (Fig. 4(a)), there is no devitrification on the SABS-0 glass powder surface, which is consistent with our observation before [30]. This means the SABS-0 glass surface is thermally stable for at least 200 h at 800 °C. When the sample is thermally treated in air at 800 °C for 500 h (Fig. 4(b)), very limited devitrification appears on the SABS-0 powder surface. This means crystalline phase(s) starts to form on the SABS-0 particle surfaces even though the nucleation sites are far from each other. After 1000 h of thermal treatment (Fig. 4(c)), visible devitrification is present on the particle surface, a reflection of the crystalline phase growth with extended thermal treatment time at 800 °C.

For the SABS-0 glass powders thermally treated in the H_2/H_2O atmosphere for 200–500 h, no surface devitrification is observed and the images are not shown here for brevity. Even after 1000 h of thermal treatment in the H_2/H_2O atmosphere, the SABS-0 glass shows little devitrification (Fig. 4(d)). This can be understood from two folds. On one hand, water vapor has a tendency to interact with the SABS-0 glass network. On the other hand, the reducing H_2/H_2O atmosphere has a tendency to inhibit the formation of the species that participate in the devitrification, such as by reducing the participating oxide species. As a result of these opposite effects, the SABS-0 glass surface devitrification is hindered. The exact process of the SABS-0 glass surface evolution in the H_2/H_2O atmosphere needs to be further studied.

For the bulk microstructure of the SABS-0 powder, the resistance to devitrification drastically increases. Fig. 5 shows the cross sections of the SABS-0 glass particles after 1000 h of thermal treatment at 800 °C in air. The samples at shorter thermal treatment time exhibit the same behavior and are not shown here. Homogeneous and amorphous glass phase can be seen. No phase separation or devitrification is observed inside the glass particles (Fig. 5(b)). The only change observed is the more rounded particle shapes after 1000 h of thermal treatment (Fig. 5(a)). This is because the thermal treatment temperature (800 °C) is higher than the T_g of the SABS-0 glass, 775 °C [20]. At temperatures higher than T_g, the SABS-0 glass particles have a tendency to spherodize. However, the microstructure remains amorphous and the devitrification on the particle surface (Fig. 4(c)) does not cause interior amorphous structure devitrification.

Fig. 6 shows the cross sections of the SABS-0 glass particles after 1000 h of thermal treatment at 800 °C in the H_2/H_2O atmosphere. The glass particles are not as round as those of the air treatment condition in Fig. 5. This means spheroidization of the SABS-0 glass in the H_2/H_2O atmosphere is limited. The cause is possibly related to the species present on the glass particle surfaces under different atmospheres as discussed. X-ray photoelectron spectroscopy seems to be the necessary technique for the surface species analysis and will be pursued in future studies. Also, bright edges can be observed on or across the SABS-0 particle surfaces in Fig. 6. This means the SABS-0 glass surface has a higher tendency to interact with the H_2/H_2O atmosphere. Still, the SABS-0 particle bulk remains stable and no devitrification is observed after 1000 h of thermal treatment at 800 °C (Fig. 6(b)).

Glass microstructure stability is affected by two factors: glass network connectivity and defects. For the bulk of the SABS-0 glass

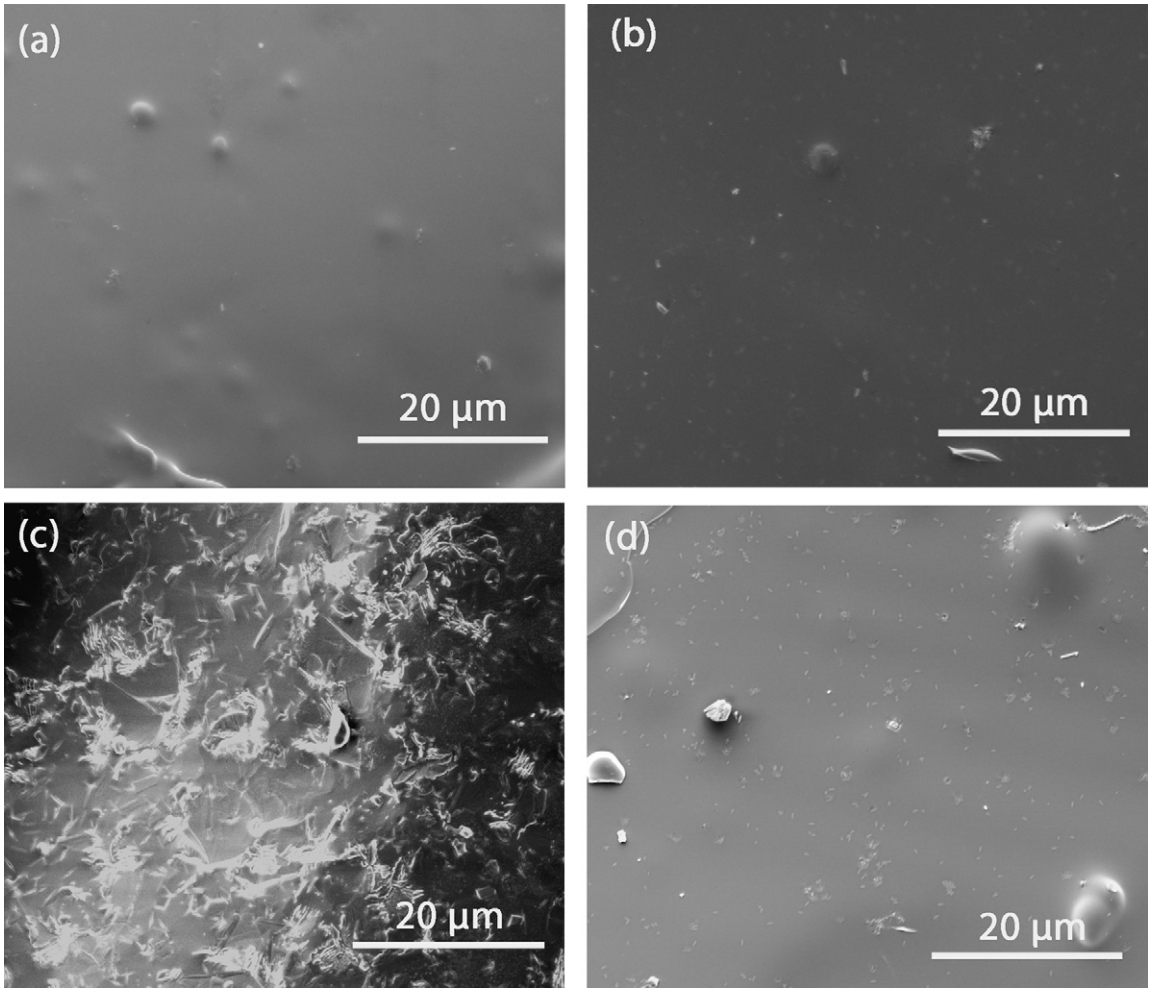

Fig. 4. SEM images of the SABS-0 glass powder surfaces after thermal treatment at 800 °C in air: (a) 200 h, (b) 500 h, and (c) 1000 h, and (d) after thermal treatment at 800 °C in H_2/H_2O for 1000 h.

powder sample, the microstructure is homogeneous and devoid of defects (scratches, dents, or tiny dust particles) or secondary species (Figs. 5, 6 and 9). The glass microstructure stability is mainly determined by the glass network connectivity. For the SABS-0 glass, the network connectivity can be quantified by measuring the non-bridging oxygen to bridging oxygen ratio from Raman spectroscopy [30]:

$$\Psi = \frac{\left[\sum Z_i(F_iV_i)/\sum Z_iV_i\right]_{\text{Network Former}}}{\left[\sum F_iV_i/\sum V_i\right]_{\text{Network Former+Modifier}}} \cdot \frac{\sum O^+}{\sum O^- + \sum O^+} \quad (2)$$

ψ is the degree of network connectivity, F_i is the field strength of oxide i in a glass system, V_i is the amount of oxide i in vol%, and Z_i is the atomic number of oxide i. The first term in Eq. (2) considers the bonding effect of cations. The second term represents the ratio of

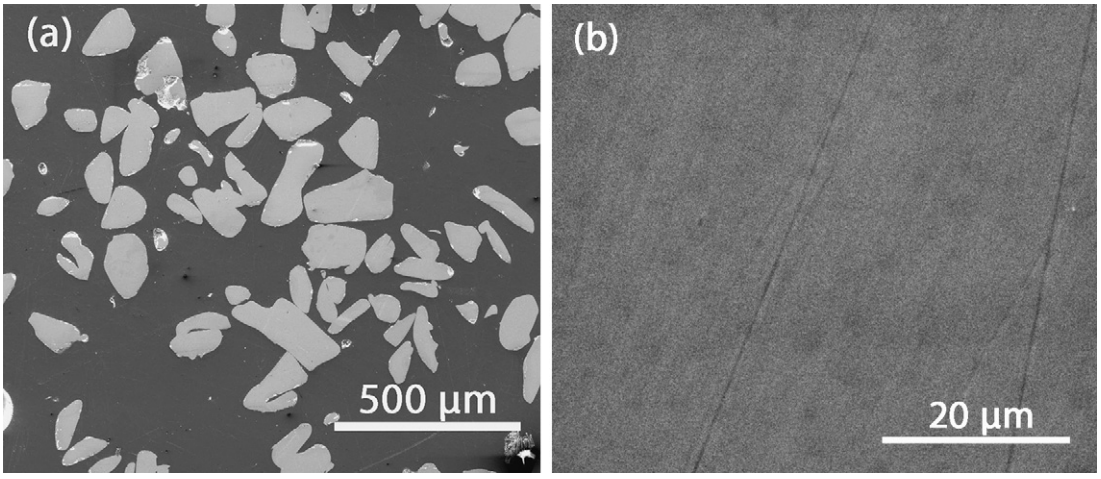

Fig. 5. SEM images of the SABS-0 glass powder cross section after thermal treatment at 800 °C in air for 1000 h.

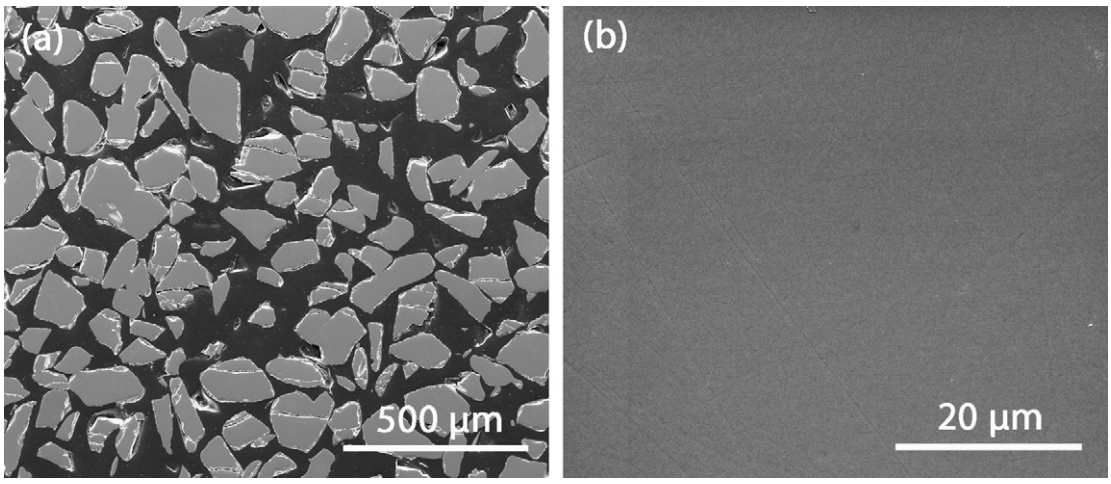

Fig. 6. SEM images of the SABS-0 glass powder cross sections after thermal treatment at 800 °C in H_2/H_2O for 1000 h.

the bridging oxygen species (O^+) vs. the total oxygen species (O^- and O^+) in a glass network. For the surface and bulk of the SABS-0 glass, the first term is the same. The key difference is the reduced amount of bridging oxygen (broken oxygen bonds) on the glass surface. For the SABS-0 glass bulk, the second term in Eq. (2) is larger, approximately by 50% by simple coordination number consideration. The SABS-0 glass surface has half of the bonds missing in comparison to the bulk. This higher bridging oxygen content in the bulk increases the glass network connectivity and thus devitrification resistance. For the SABS-0 glass, the bulk network connectivity is about 80% and thus highly stable [30]. It should be pointed out that broken oxygen bonds mainly exist on the SABS-0 glass surface, likely in <1–2 nm thickness. So the SABS-0 surface devitrification should be limited to a very thin layer, likely <2 nm. This understanding is supported by the SABS-0 glass particle cross section microstructure analysis. No crystalline layer around the SABS-0 particles can be observed from the SEM analysis, which has 2–5 nm resolution. This means the SABS-0 glass has excellent thermal stability in SOFC/SOEC operating environments and is a promising sealant material for SOFCs/SOECs.

3.3. Polished surface microstructure stability

For SOFC/SOEC applications, seal glass surface can be modified and defect sites such as scratches, dents, and solid impurities can be created before use. These sites can then act as preferential nucleation and devitrification locations and thus reduce glass thermal stability. In this study, bulk SABS-0 glass surface was polished to mimic this aspect. Fig. 7 shows the SEM images of the bulk SABS-0 glass surfaces after different thermal treatment time in air. Before the thermal treatment, the glass surface is homogeneous; no devitrified phase can be seen at both low and high magnifications except for a few defects (Fig. 7(a) and (b)). For the 200 h thermally treated sample (Fig. 7(c) and (d)), some dark and round-shaped spots with 2–3 μm size appear on the surface. Crescent-shaped crystallites arise from these spots. For the 500 h thermally treated sample (Fig. 7(e) and (f)), the amount of crystalline phase(s) drastically increases. At low magnification (Fig. 7(e)), it shows that the crescent-shaped crystallites break into individual nuclei. There is substantial crystal growth and needle-shaped crystals with 300–400 nm length appear over the phase-separated regions for the whole sample surface (Fig. 7(f)). For the regions outside of the initial phase-separated dark spots, the amount of the crystalline phase(s) is much less. For the 1000 h thermally treated samples (Fig. 7(g) and (h)), the surface is fully covered with crystalline phase(s); the dark and light phase regions are not distinguishable anymore. The needle-shaped crystalline phase(s) grow to ~1 μm size and prismatic shape.

Fig. 8 shows the SEM images of the SABS-0 bulk glass surfaces after different thermal treatment time in the H_2/H_2O atmosphere. The surfaces of the SABS-0 bulk samples generally show the same microstructures as those treated in the air atmosphere. However, phase separation and devitrification occur much earlier, only after 100 h of thermal treatment (Fig. 8(a) and (b)). The appearance and break-up of the crescent-shaped crystallites are not captured. This means the H_2/H_2O atmosphere has a higher tendency of inducing SABS-0 devitrification. After 200 h of thermal treatment, devitrification increases and the devitrified phase(s) distributes evenly on the SABS-0 glass surface (Fig. 8(c) and (d)) in comparison to the localized distribution in the phase-separated regions in Fig. 7(c) and (d) for the air treated condition. The devitrified crystallites are twice the size of the 500 h thermally treated sample in air, at ~250 nm (Fig. 8(c) and (d) vs. Fig. 7(e) and (f)). As the thermal treatment time increases to 500 h and 1000 h, the needle-shaped crystallites keep growing for the whole sample surface (Fig. 8(e)–(h)). However, the final crystallite sizes are smaller than those of the corresponding air treatment conditions. This interesting crystallite size reversal can be explained from the number density of the devitrified crystallites point of view. The air treated SABS-0 sample has much lower crystallite number density (Fig. 7(c) and (d)) than that of the H_2/H_2O atmosphere treated sample (Fig. 8(c) and (d)). For the former, the crystallites can grow more extensively before impinging each other. For the latter, more crystallites are present for a given area and constrained from growing into large sizes. Because of this impingement factor, the final crystallite shape for the H_2/H_2O atmosphere treatment condition remains rod-like (Fig. 8(h)) instead of the much larger prismatic shape for the air treated sample (Fig. 7(h)).

After the nucleation of the devitrified phase(s), crystal growth is a three-dimensional event and spreads over the SABS-0 glass surface and towards its interior. At a critical point, further growth on the surface is inhibited because of the crystal impingement. Crystallites only grow towards the SABS-0 glass interior. The time from lateral growth to depth growth can be expressed as [31]:

$$t_m = \frac{1}{2\mu\sqrt{N_s}} \tag{3}$$

t_m is the crystallization kinetic change from lateral growth to depth growth. N_s is the areal number density of nucleation sites, and μ is crystal/glass boundary moving velocity. Around the defect sites, new crystallites are limited from growing into large sizes because of the early impingement due to their higher number density. For the

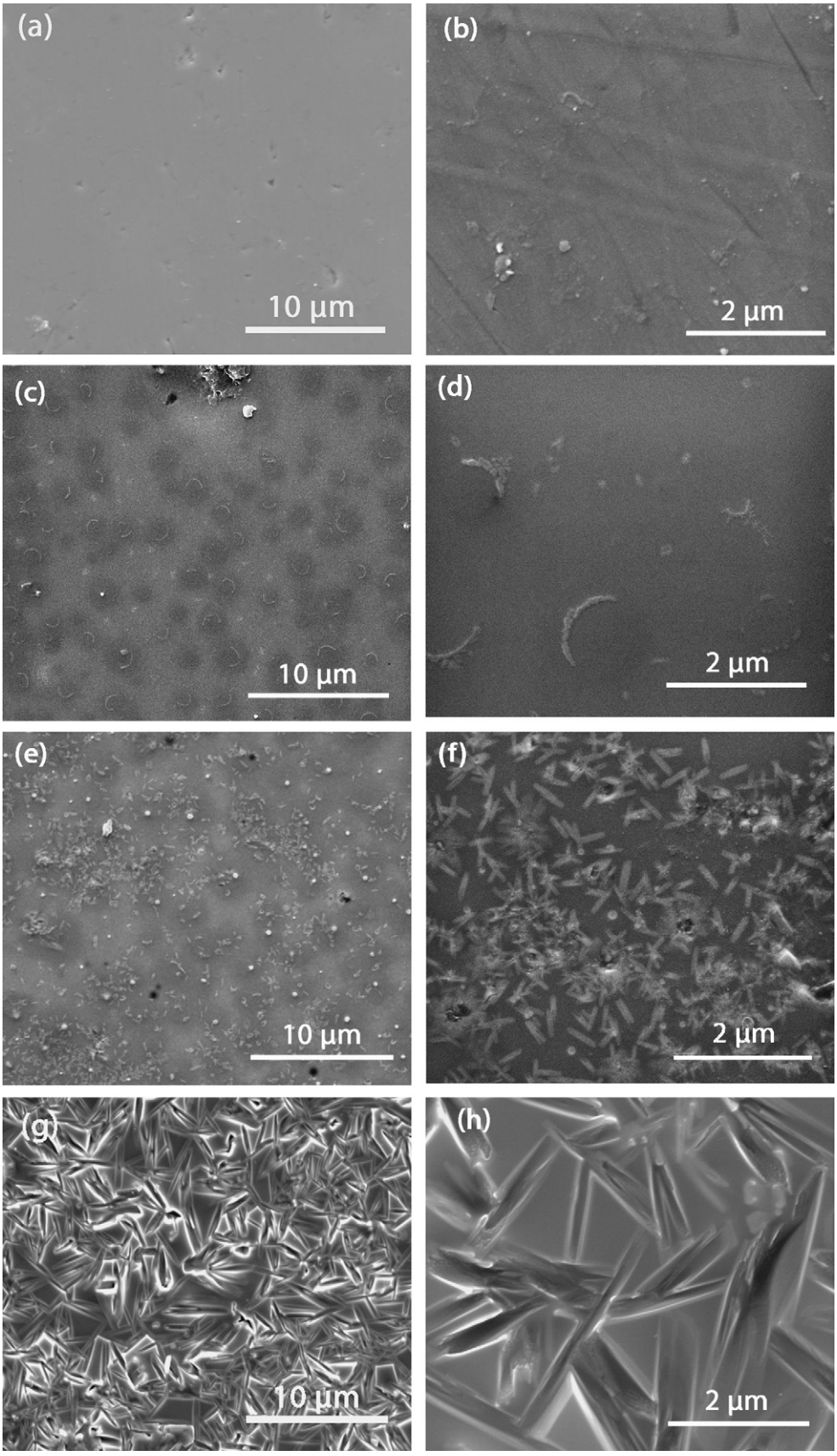

Fig. 7. SEM images of SABS-0 bulk glass surfaces before thermal treatment and after thermally treated at 800 °C in air: (a) and (b) as polished, (c) and (d) 200 h, (e) and (f) 500 h, (g) and (h) 1000 h.

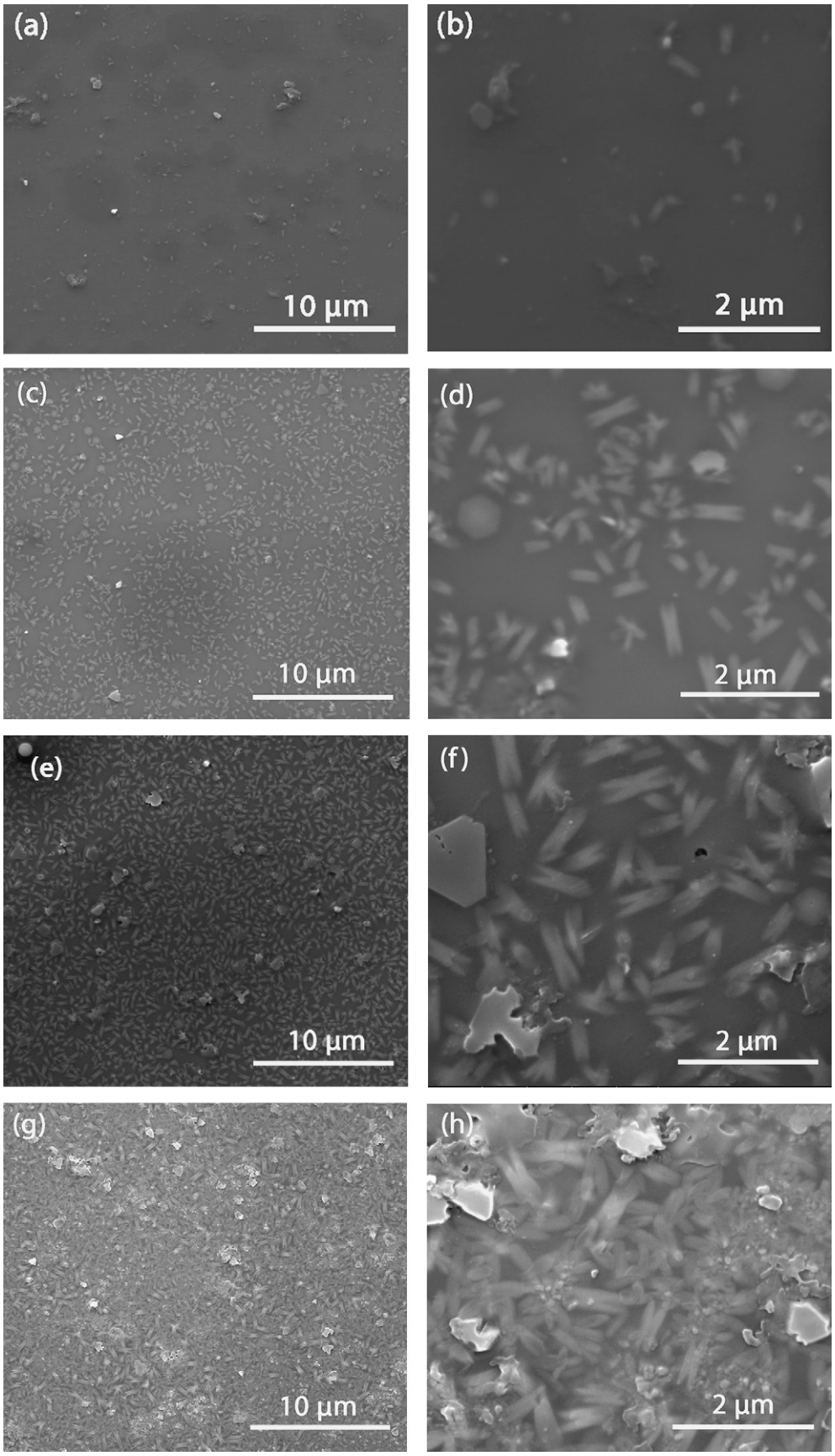

Fig. 8. SEM images of polished SABS-0 bulk glass surfaces after thermally treated at 800 °C in the H_2/H_2O atmosphere: (a) and (b) 100 h, (c) and (d) 200 h, (e) and (f) 500 h, (g) and (h) 1000 h.

defect-free regions, the crystallites form at a later stage and have a lower number density. Crystal growth is relatively un-hindered and the crystallite sizes are much larger. However, the above observation is made based on the observations from the glass surface. It is possible that the crystals in the regions of higher number density have grown more in the depth direction. This is difficult to analyze because the devitrified layer is three-dimensional in nature but at the same time very thin. However, it can be envisioned that as the thermal treatment continues, the depth direction growth will slow down because the diffusion distance for the crystalline species becomes longer.

Several fundamental observations can be made from the devitrification process in Figs. 7 and 8. At the initial stage, the events are mainly driven by thermodynamics. This includes phase separation, nucleation, and break-up of the crescent-shaped new crystallites. The number density of the nucleation sites is non-uniform on the SABS-0 glass surface. Nucleation initiates randomly but preferentially around the surface defects. If the nucleation process is fast enough (such as for the H_2/H_2O atmosphere case), the nucleation sites will distribute more homogeneously. At the later stage of the devitrification process, thermodynamics still drives the fundamental devitrification process but kinetics becomes the limiting factor. This involves nuclei areal density effect on crystal growth rate, crystallite size, and growth direction. The crystallite size difference can reverse and the crystal shape can be different for different atmospheres at the same thermal treatment time. However, it is difficult to predict final crystallite sizes because new crystalline formation continues while the existing crystallites grow.

Comparing Figs. 7 and 8, an additional factor to consider is the atmosphere effect on polished surface devitrification. The H_2/H_2O atmosphere is more likely to induce devitrification for the polished SABS-0 glass surface. The fundamental cause is believed to be mainly from water [32]. H_2 involvement in the SABS-0 glass microstructure is minimal. Water dissociates into hydroxyl (OH^-) groups, penetrates into the surface layer of the Si–O lattice, breaks the Si–O–Si network, and forms siloxane Si–OH bonds [33–37]:

$$\text{Si–O–Si} + H_2O \rightarrow \text{Si–OH} + \text{HO–Si} \quad (4)$$

Even though the amount of $Si(OH)_x^{4-x}$ species is low and no measureable weight change is detected, its impact on the glass network connectivity is significant. With the decrease of the glass network connectivity and the increase of the amount of $Si(OH)_x^{4-x}$ structural units, local microheterogeneity and broken glass network from polishing lead to surface devitrification. For the air treatment condition, water content is much lower and the surface devitrification process is hindered.

3.4. Glass phase stability

Fig. 9 shows the XRD patterns of the SABS-0 powder samples after the thermal treatment at 800 °C in air. There is no crystalline peak for the samples thermally treated for 200, 500, and 1000 h. This result indicates that the SABS-0 glass is very stable at 800 °C and remains amorphous. Devitrification seen in Fig. 4 only occurs on the very surface of the SABS-0 particles. The devitrified phase volume is negligible compared to the amorphous phase volume.

For the thermal treatment in the H_2/H_2O atmosphere, the SABS-0 glass powder remains amorphous for up to 1000 h. Fig. 9 only shows the XRD pattern of the 1000 h thermally treated SABS-0 glass powder for brevity. This means the H_2/H_2O atmosphere poses no significant effect on the SABS-0 glass bulk structure stability.

Fig. 10 shows the XRD patterns of the polished SABS-0 bulk glass surfaces at as-polished condition and after different thermal treatment times in air. Consistent with the microstructure results (Fig. 7), devitrification takes place on the SABS-0 bulk glass surface and increases with thermal treatment time. Although X-ray penetrates into the bulk glass, 90% of the signals are collected from less than 25 μm depth. This means polishing induces devitrification on the SABS-0 glass surface and causes instability of the glass. Energy dispersive spectroscopy (EDS) spot analysis shows that the devitrified regions are Si, Sr, and Al rich. XRD analysis shows that the new crystalline phases are Al_2SiO_5, Sr_2SiO_4, and $Sr_7Al_{12}O_{25}$. The devitrification process can be understood as follows. In the SABS-0 glass, SiO_2 is a glass former. SrO is a glass modifier and charge compensator for the nearest Si_2O_5, Si_2O_6, Si_2O_7, and SiO_4 structural units. Al_2O_3 is an intermediate and can be a network former or a network modifier. Microheterogeneity in the SABS-0 glass arises due to 'local ordering' of the glass structural units. As a result, Sr_2SiO_4, Al_2SiO_5, and $Sr_7Al_{12}O_{25}$ phases form. In Fig. 10, polishing alone creates minor peaks on the XRD spectrum. As the thermal treatment time increases, the XRD peaks evolve. This demonstrates that polishing and thermal treatment are dynamic processes for crystalline phase formation. The stress concentration sites and defects on the SABS-0 surface from polishing preferentially act as devitrification

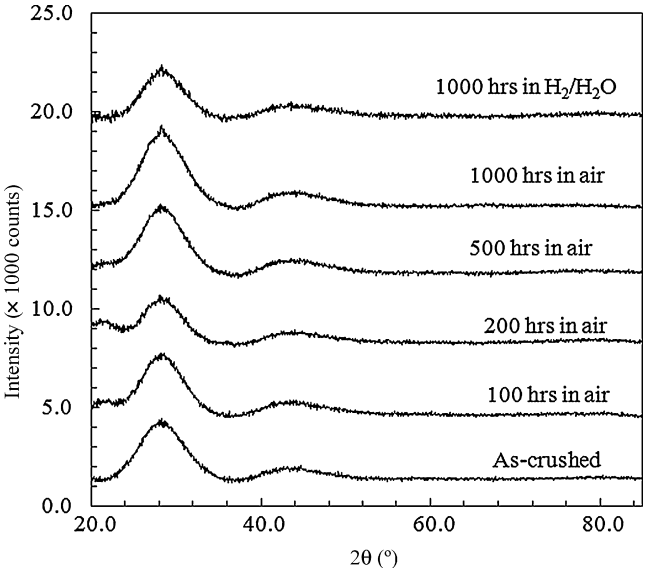

Fig. 9. XRD patterns of the SABS-0 glass powders thermally treated at 800 °C in air for different times and thermally treated at 800 °C in the H_2/H_2O atmosphere for 1000 h.

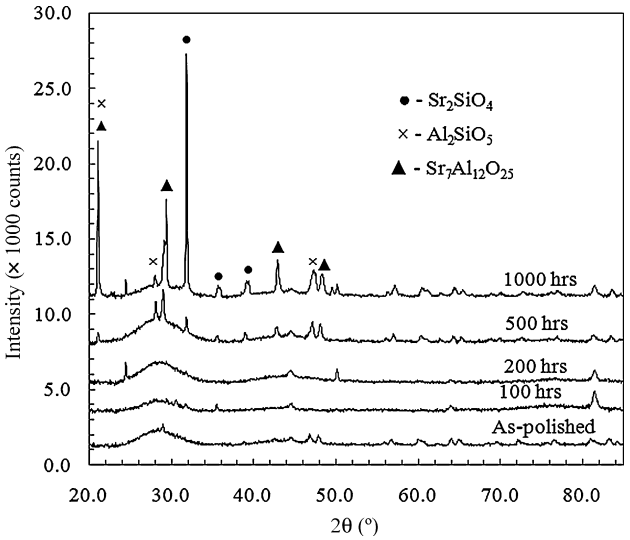

Fig. 10. XRD patterns of the SABS-0 bulk glass polished surfaces thermally treated at 800 °C for different times in air.

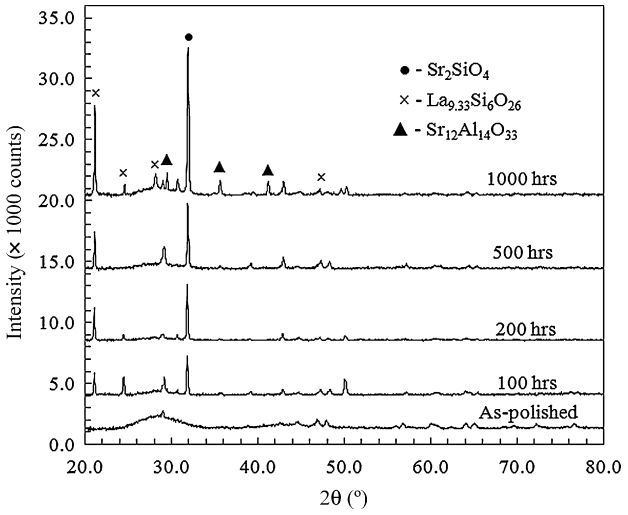

Fig. 11. XRD patterns of the SABS-0 bulk glass polished surfaces thermally treated at 800 °C for different times in the H_2/H_2O atmosphere.

sites. At short thermal treatment time, these defects induce new phase formation even though the new phase may not be stable. As the thermal treatment time increases, the new phase(s) evolves into relatively stable species. The peaks from the devitrified phases become stronger with the thermal treatment time. For the 200 h thermal treatment time, the crystalline peaks are weak. After 500 h of thermal treatment time, devitrification becomes more obvious; needle-shaped crystals can be seen in Fig. 7(f). For the 1000 h thermal treatment sample, diffraction peaks are several times stronger than those of the 500 h thermally treated sample and more peaks are present (Fig. 10); devitrification happens more extensively from 500 to 1000 h thermal treatment time (Fig. 7(g) and (h)).

Fig. 11 shows the XRD patterns of the SABS-0 bulk glass sample surface after different thermal treatment times in the H_2/H_2O atmosphere. The devitrified phases are Sr_2SiO_4, $La_{9.33}Si_6O_{26}$, and $Sr_{12}Al_{14}O_{33}$. The phase evolution process can be explained similar to the air treatment case. However, the peaks appear much earlier, such as after 100 h of thermal treatment, consistent with the observation in Fig. 8(a) and (b). After 1000 h of thermal treatment, however, the air treatment condition shows higher number and intensity of devitrification peaks (Fig. 10 vs. Fig. 11). This means the H_2/H_2O atmosphere increases the devitrification tendency of the SABS-0 glass initially even though it does not lead to higher content of new phase(s) at prolonged thermal treatment time. The XRD pattern reversal is consistent with the microstructural results.

4. Conclusion

Thermal stability of a novel B_2O_3 free $SrO–La_2O_3–Al_2O_3–SiO_2$ glass (SABS-0) as a SOFC/SOEC sealant is evaluated in both air and H_2/H_2O atmospheres at 800 °C for up to 1000 h. Weight change is negligible under all the thermal treatment conditions. The SABS-0 glass bulk remains amorphous after thermal treatment for 1000 h in both atmospheres. Devitrification is only observed on the very surface of the SABS-0 glass under both atmospheres. Polishing accelerates the SABS-0 glass surface devitrification. The H_2/H_2O atmosphere induces earlier surface devitrification but the final extent of devitrification is more limited. The crystal phases are identified as Sr_2SiO_4, Al_2SiO_5, and $Sr_7Al_{12}O_{25}$ for the air treatment condition and Sr_2SiO_4, $La_{9.33}Si_6O_{26}$, and $Sr_{12}Al_{14}O_{33}$ for the H_2/H_2O thermal treatment condition. The study demonstrates that the SABS-0 glass has excellent thermal stability in SOFC/SOEC operating environments and is a promising sealant material for SOFCs/SOECs.

Acknowledgments

This material is based on work supported by Department of Energy under Award Number DE-FC07-06ID14739. The SEM analysis was done in Nanoscale Characterization and Fabrication Laboratory of Virginia Tech.

References

[1] L. Peng, Q.S. Zhu, Z.H. Xie, W.L. Huang, J. Inorg. Mater. 21 (2006) 867–872.
[2] P.A. Lessing, J. Mater. Sci. 42 (2007) 3465–3476.
[3] J.W. Fergus, J. Power Sources 147 (2005) 46–57.
[4] EG&G Technical Services, Fuel Cell Handbook, 7th ed., US Department of Energy, Office of Fossil Energy, National Energy Technology Laboratory, 2004.
[5] S.C. Singhal, K. Kendall, High Temperature Solid Oxide Fuel Cells, Elsevier, Oxford, UK, 2003.
[6] K.S. Weil, JOM 58 (2006) 37–44.
[7] T. Kawada, T. Horita, N. Sakai, H. Yokokawa, M. Dokiya, J. Mizusaki, Solid State Ionics 131 (2000) 199–210.
[8] K.L. Ley, M. Krumpelt, R. Kumar, J.H. Meiser, J. Bloom, J. Mater. Res. 11 (1996) 1489–1493.
[9] C. Lara, M.J. Pascual, M.O. Prado, A. Duran, Solid State Ionics 170 (2004) 201–208.
[10] N.P. Bansal, E.A. Gamble, J. Power Sources 147 (2005) 107–115.
[11] K.D. Meinhardt, D.S. Kim, Y.S. Chou, K.S. Weil, J. Power Sources 182 (2008) 188–196.
[12] M. Brochu, B.D. Gauntt, R. Shah, G. Miyake, R.E. Loehman, J. Eur. Ceram. Soc. 26 (2006) 3307–3313.
[13] A. Flugel, M.D. Dolan, A.K. Varshneya, Y. Zheng, N. Coleman, M. Hall, D. Earl, S.T. Misture, J. Electrochem. Soc. 154 (2007) B601–B608.
[14] S. Ghosh, P. Kundu, A.D. Sharma, R.N. Basu, H.S. Maiti, J. Eur. Ceram. Soc. 28 (2008) 69–76.
[15] S.B. Sohn, S.Y. Choi, G.H. Kim, H.S. Song, G.D. Kim, J. Am. Ceram. Soc. 87 (2004) 254–260.
[16] K. Eichler, G. Solow, P. Otschik, W. Schaffrath, J. Eur. Ceram. Soc. 19 (1999) 1101–1104.
[17] T. Zhang, W.G. Fahrenholtz, S.T. Reis, R.K. Brow, J. Am. Ceram. Soc. 91 (2008) 2564–2569.
[18] F. Smeacetto, M. Salvo, M. Ferraris, J. Cho, A.R. Boccaccini, J. Eur. Ceram. Soc. 28 (2008) 61–68.
[19] M.K. Mahapatra, K. Lu, W.T. Reynolds Jr., J. Power Sources 179 (2008) 106–112.
[20] M.K. Mahapatra, K. Lu, R.J. Bodnar, Appl. Phys. A 95 (2009) 493–500.
[21] M.K. Mahapatra, K. Lu, J. Power Sources 185 (2008) 993–1000.
[22] J. Schmelzer, R. Pascova, J. Moller, I. Gutzow, J. Non-Cryst. Solids 162 (1993) 26–39.
[23] J.R. Mawdsley, J.D. Carter, A.J. Kropf, B. Yildiz, V.A. Maroni, Int. J. Hydrogen Energy 34 (2009) 4198–4207.
[24] N.H. Menzler, D. Sebold, M. Zahid, S.M. Gross, T. Koppitz, J. Power Sources 152 (2005) 156–167.
[25] R.K. Brow, S.T. Reis, T. Zhang, Office of Fossil Energy Fuel Cell Program Annual Report, August 2007, pp. 132–134.
[26] R. Loehman, E. Corral, M. Chavez, Office of Fossil Energy Fuel Cell Program Annual Report, August 2007, pp. 113–117.
[27] R.N. Singh, Office of Fossil Energy Fuel Cell Program Annual Report, August 2007, pp. 126–128.
[28] E. Wittman, E.D. Zanotto, J. Non-Cryst. Solids 271 (2000) 94–99.
[29] P. Pernice, S. Esposito, A. Aronne, V.N. Sigaev, J. Non-Cryst. Solids 258 (1999) 1–10.
[30] K. Lu, M.K. Mahapatra, J. Appl. Phys. 104 (2008) 074910-1–074910-9.
[31] E.B. Ferreira, M.L.F. Nascimento, H. Stoppa, E.D. Zanotto, Eur. J. Glass Sci. Technol. B 49 (2008) 81–89.
[32] C.S. Ray, W.H. Huang, D.E. Day, J. Am. Ceram. Soc. 74 (1991) 60–66.
[33] Y. Moriya, M. Nogami, J. Non-Cryst. Solids 38/39 (1980) 667–672.
[34] M. Tomozawa, J. Non-Cryst. Solids 73 (1985) 197–204.
[35] S. Fujita, A. Sakamoto, M. Tomozawa, J. Non-Cryst. Solids 320 (2003) 56–63.
[36] G. Perera, R.H. Doremus, W. Lanford, J. Am. Ceram. Soc. 74 (1991) 1269–1274.
[37] W. Liang, G.R. Chen, J.J. Cheng, M.F. Zhou, Glass Technol. 40 (1999) 184–186.